International Journal of Solids and Structures 47 (2010) 2178–2189

Contents lists available at ScienceDirect

International Journal of Solids and Structures

journal homepage: www.elsevier.com/locate/ijsolstr

An interaction integral method for 3D curved cracks in nonhomogeneous materials with complex interfaces

Hongjun Yu [a,*], Linzhi Wu [a,**], Licheng Guo [a], Huaping Wu [b], Shanyi Du [a]

[a] Center for Composite Materials, Harbin Institute of Technology, Harbin 150001, China
[b] Key Laboratory of Special Purpose Equipment and Advanced Processing Technology (Zhejiang University of Technology), Ministry of Education, 310032, China

ARTICLE INFO

Article history:
Received 1 December 2009
Received in revised form 28 March 2010
Available online 28 April 2010

Keywords:
Interaction integral
Stress intensity factors (SIFs)
Three-dimensional (3D)
Nonhomogeneous materials
Interface
Finite element method (FEM)

ABSTRACT

This work derives an interaction integral for the computation of mixed-mode stress intensity factors (SIFs) in three-dimensional (3D) nonhomogeneous materials with continuous or discontinuous properties. The present method is based on a two-state integral by the superposition of actual and auxiliary fields. In 3D domain formulation of the interaction integral derived here, the integrand does not involve any derivatives of material properties. Furthermore, the formulation can be proved to be still valid even when the integral domain contains material interfaces. Therefore, it is not necessary to limit the material properties to be continuous for the present formulation. On account of these advantages, the application range of the interaction integral can be greatly enlarged. This method in conjunction with the finite element method (FEM) is employed to solve several representative fracture problems. According to the comparison between the results and those from the published lectures, good agreement demonstrates the validation of the interaction integral. The results show that the present interaction integral is domain-independent for nonhomogeneous materials with interfaces.

1. Introduction

Recently, composite materials and structures are more and more designed and produced with nonhomogeneous properties. Some of them have the properties varying continuously and some of them contain large number of interfaces. For there-dimensional (3D) curved cracks in those materials and structures, the accurate determination of mixed-mode stress intensity factors (SIFs) remains a significant problem in fracture mechanics. Irwin (1962) first obtained an approximate solution of a semi-elliptical surface crack problem in a homogeneous infinite plate. Then, Smith et al. (1967), Smith (1972) and Shah and Kobayashi (1972) refined the accuracy of the SIFs for this problem using the iteration method. Raju and Newman (1979) employed finite element techniques to analyze the problems on semi-elliptical surface cracks in finite-thickness plates. The problems of a penny-shaped crack in homogeneous dissimilar materials bonded through an interfacial region with graded mechanical properties were investigated by Ozturk and Erdogan (1996). An alternative approach for analyzing 3D curved cracks in homogeneous and functionally graded materials (FGMs, which are the nonhomogeneous materials with properties varying continuously) is to directly include the SIFs as unknowns in the finite element displacement approximation (Ayhan and Nied, 2002; Ayhan, 2007, 2009). Yildirim et al. (2005) employed the displacement correlation technique (DCT) in conjunction with the finite element method (FEM) to examine 3D surface crack problems in functionally graded coatings subjected to mode-I mechanical or transient thermal loading. Yu et al. (2007) used the DCT to solve 3D rectangular penetrable crack problems in functionally graded plates.

In recent decades, conservation integrals have been widely applied to solve the SIFs, among which the J-integral (Rice, 1968) has aroused a great interest for its path-independence in homogeneous materials. It is well-known that the J-integral is identical to energy release rate corresponding to the extension of a crack in an elastic body (Moran and Shih, 1987b). Under some restrictive conditions, DeLorenzi (1982) derived a domain form of the J-integral along a 3D crack front. Shih et al. (1986) employed the domain integral to investigate 3D cracks in a thermally stressed body. In several applications, the contour integrals and their associated domain formulations have been investigated by Moran and Shih (1987a,b). They pointed out that due to the potential source of inaccuracy for the evaluation of the crack tip contour integrals in numerical studies, the integrals should be recast into finite domain forms with the help of weighting functions. Based on the FEM coupled with the element-free Galerkin method (EFGM), Sukumar et al. (1997) employed a 3D domain formulation of the J-integral to analyze 3D planar crack problems. With the development of the extended finite element method (XFEM), Sukumar et al. (2000) implemented the J-integral in conjunction with the XFEM to solve

* Corresponding author. Tel.: +86 451 86402376; fax: +86 451 86402386.
** Corresponding author. Tel.: +86 451 86402376; fax: +86 451 86402386.
E-mail addresses: yuhongjun@hit.edu.cn (H. Yu), wlz@hit.edu.cn (L. Wu).

0020-7683/$ - see front matter © 2010 Elsevier Ltd. All rights reserved.
doi:10.1016/j.ijsolstr.2010.04.027

3D planar crack problems. Eischen (1987) proved that in nonhomogeneous materials with continuous and generally differentiable properties, the stress and strain singularity near a crack tip is same as the well-known inverse square root stress singularity in homogeneous materials. And Jin and Sun (2007) provided a rigorous proof for nonhomogeneous materials that both the modified J-integral given by Eischen (1987) and the J_e-integral given by Honein and Herrmann (1997) are the potential energy release rates. These studies permit the application of the J-integral in fracture problems of nonhomogeneous materials with properties varying continuously. Walters et al. (2004) used the domain form of the J-integral as well as the DCT to compute the SIFs of semi-elliptical surface cracks in FGM plates under mode-I thermomechanical loading.

In order to obtain mode-I and mode-II SIFs separately, an interaction (energy) contour integral method (Stern et al., 1976) is derived from the traditional J-integral by considering a composition of two admissible states (actual and known auxiliary fields). Wang et al. (1980) introduced this method to study two-dimensional (2D) mixed-mode crack problems in rectilinear anisotropic solids. Nakamura (1991) used an equivalent domain expression of the interaction integral to evaluate mixed-mode SIFs along straight 3D interface cracks. The same method was employed to deal with curved 3D interface crack problems (Nahta and Moran, 1993; Gosz et al., 1998). Krysl and Belytschko (1999) utilized the interaction integral method in conjunction with the EFGM to investigate 3D stationary and propagating crack problems. Kim et al. (2001) employed the method to extract mixed-mode SIFs along a penny-shaped crack front. Gosz and Moran (2002) developed the interaction integral method for non-planar 3D crack problems. Moës et al. (2002) and Gravouil et al. (2002) used the method combined with the XFEM to study non-planar 3D crack growth problems. Furthermore, Dolbow and Gosz (2002) introduced the interaction integral method to compute mixed-mode SIFs of 2D cracks in FGMs. In comparison with the modified J-integral for nonhomogeneous materials, the interaction integral was found to be more convenient since the evaluation of strain energy densities along the traction-free crack faces is not required. According to a series of investigations (Kim and Paulino, 2003, 2004, 2005), Kim and Paulino gave a systemical summary on three definitions of the auxiliary fields and discussed how to extract mixed-mode SIFs and T-stress of 2D cracks in isotropic and orthotropic FGMs. Using the method, Walters et al. (2005, 2006) conducted several investigations on 3D mixed-mode fracture problems for FGMs under thermomechanical loads. Ortiz and Cisilino (2005) determined mixed-mode SIFs along 3D bimaterial interface crack fronts using the interaction integral method in conjunction with the boundary element method (BEM). Johnson and Qu (2007) extended the interaction integral method to calculate the SIFs of 3D curved cracks in a homogeneous body and on a bimaterial interface subjected to non-uniform temperature fields.

The previous work is mostly concerned with the materials with continuous and differentiable properties. Actually, there exist more or less material interfaces in various nonhomogeneous composite materials, especially, in particulate reinforced composite materials (PRCMs). It is often found that although the PRCMs can significantly improve the strength, stiffness and wear resistance of the structures (Leggoe et al., 1996), their fracture properties are not improved and, on the contrary, the fracture toughness may be significantly lower than that of the matrix material (Yang and Li, 2004). In addition, FGMs as typical nonhomogeneous materials have many advantages that make them attractive in potential applications, such as the improvement on residual stress distribution and mechanical durability, while actual FGMs are also two or multi-phase particulate composites in which material composition and microstructure vary spatially (Rahman and Chakraborty, 2007) or the volume fraction of particles varies in one or several directions (Birman and Byrd, 2007). Therefore, the material interfaces have to be taken into account if the fracture performance of these materials must be concerned. In authors' previous work (Yu et al., 2009), the interaction integral method was extended to solve the fracture problems in 2D nonhomogeneous materials with complex interfaces. It has been proved that the interaction integral is still valid when the integral domain contains material interfaces. In this paper, the applications of the interaction integral will be discussed for 3D curved cracks in nonhomogeneous materials when the integral domain contains arbitrary interfaces.

The outline of this paper is given as follows. An interaction integral and the method for extracting mixed-mode SIFs are given in Section 2. Moreover, Section 2 provides the derivation of the 3D domain form of the interaction integral which does not contain the derivatives of material properties. Section 3 gives the proof that the interaction integral method is still valid when there are arbitrarily curved interfaces in the integral domain. Section 4 presents several representative numerical examples to demonstrate the validation of the interaction integral and verify the domain-independence for the materials with properties varying continuously and those with complex interfaces. Finally, a summary is provided in Section 5.

2. Interaction integral

In this section, the interaction integral will be derived for extracting mixed-mode SIFs along 3D curved crack fronts in arbitrarily nonhomogeneous solids. Throughout this work, the material is limited to linear-elastic and isotropic conditions, and small strain kinematics is assumed.

2.1. Interaction energy contour integral

Fig. 1 shows an arbitrary 3D curved crack front. Here, $\Gamma(s)$ is a contour that lies in a plane passing through the point s and is perpendicular to the crack front, n_j are the components of the unit outward normal to the contour Γ. According to Gosz and Moran (2002), the pointwise energy release rate at point s takes the form

$$J(s) = \lim_{\Gamma \to 0} c_l(s) \int_{\Gamma(s)} (W\delta_{lj} - u_{i,l}\sigma_{ij}) n_j \, d\Gamma \tag{1}$$

where $W = \frac{1}{2}\sigma_{ij}\varepsilon_{ij} = \frac{1}{2}C_{ijkl}\varepsilon_{ij}\varepsilon_{kl} = \frac{1}{2}S_{ijkl}\sigma_{ij}\sigma_{kl}$ is the strain energy density, σ_{ij} is the Cauchy stress tensor, ε_{ij} is the strain tensor, u_i is the displacement vector, C_{ijkl} is the stiffness tensor, S_{ijkl} is the compliance tensor, δ_{lj} is the Kronecker delta, and $c_l(s)$ is a unit vector that is perpendicular to the crack front and lies in the local tangent plane to the crack surface at point s. Without specification, the variables

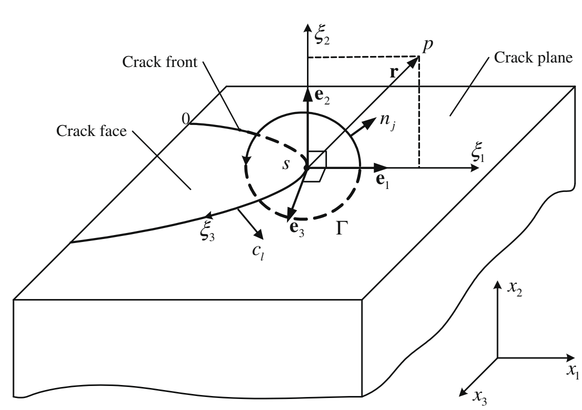

Fig. 1. Schematic of a curved crack front and related curvilinear coordinate system.

marked by the subscripts i, j, k and l denote their components in the Cartesian coordinate system. Throughout, the summation convention is implied where the subscripts take on the values 1–3. The comma denotes partial differentiation with respect to the spatial coordinates.

The J-integral (Rice, 1968) for the superimposed load of the actual field and the auxiliary field can be written as

$$J^S(s) = \lim_{\Gamma\to 0} c_l(s) \int_{\Gamma(s)} \left[\frac{1}{2}\left(\sigma_{ik} + \sigma_{ik}^{\mathrm{aux}}\right)\left(\varepsilon_{ik} + \varepsilon_{ik}^{\mathrm{aux}}\right)\delta_{lj} - \left(u_{i,l} + u_{i,l}^{\mathrm{aux}}\right)\left(\sigma_{ij} + \sigma_{ij}^{\mathrm{aux}}\right)\right] n_j \, d\Gamma \tag{2}$$

where $\sigma_{ij}^{\mathrm{aux}}$, $\varepsilon_{ij}^{\mathrm{aux}}$ and u_i^{aux} are the auxiliary stress, strain and displacement fields defined in Appendix A. The interaction integral (Stern et al., 1976) is the interactional part of actual and auxiliary fields in the integral $J^s(s)$, that is

$$I(s) = \lim_{\Gamma\to 0} c_l(s) \int_{\Gamma(s)} \left[\frac{1}{2}\left(\sigma_{ik}\varepsilon_{ik}^{\mathrm{aux}} + \sigma_{ik}^{\mathrm{aux}}\varepsilon_{ik}\right)\delta_{lj} - u_{i,l}\sigma_{ij}^{\mathrm{aux}} - u_{i,l}^{\mathrm{aux}}\sigma_{ij}\right] n_j \, d\Gamma \tag{3}$$

According to the definition of the auxiliary fields, $\sigma_{ij}\varepsilon_{ij}^{\mathrm{aux}} = \sigma_{ij}S_{ijkl}(\mathbf{x})\sigma_{kl}^{\mathrm{aux}} = \sigma_{kl}^{\mathrm{aux}}\varepsilon_{kl}$, and hence, Eq. (3) can be rewritten as

$$I(s) = \lim_{\Gamma\to 0} c_l(s) \int_{\Gamma(s)} P_{lj} n_j \, d\Gamma \tag{4}$$

where

$$P_{lj} = \sigma_{ik}^{\mathrm{aux}}\varepsilon_{ik}\delta_{lj} - u_{i,l}\sigma_{ij}^{\mathrm{aux}} - u_{i,l}^{\mathrm{aux}}\sigma_{ij} \tag{5}$$

2.2. Extraction of mixed-mode SIFs from the interaction integral

Similarly to the relations between the energy release rate $J(s)$ and the SIFs K_{I}, K_{II} and K_{III}, the interaction integral $I(s)$ in Eq. (4) takes the value (Walters et al., 2006)

$$I(s) = \frac{2}{E'(s)}\left(K_{\mathrm{I}}K_{\mathrm{I}}^{\mathrm{aux}} + K_{\mathrm{II}}K_{\mathrm{II}}^{\mathrm{aux}}\right) + \frac{1}{\mu(s)}K_{\mathrm{III}}K_{\mathrm{III}}^{\mathrm{aux}} \tag{6}$$

where $E'(s) = E(s)$ for plane stress, $E'(s) = E(s)/[1 - \nu^2(s)]$ for plane strain and $\mu(s) = E(s)/[2 + 2\nu(s)]$ is shear modulus. Substituting the auxiliary SIFs $K_{\mathrm{I}}^{\mathrm{aux}} = 1$ and $K_{\mathrm{II}}^{\mathrm{aux}} = K_{\mathrm{III}}^{\mathrm{aux}} = 0$ into Eq. (6), we can get the value of $K_{\mathrm{I}}(s)$ from the integral $I(s)$. Similarly, $K_{\mathrm{II}}(s)$ and $K_{\mathrm{III}}(s)$ can also be obtained from Eq. (6) by setting $K_{\mathrm{II}}^{\mathrm{aux}} = 1$, $K_{\mathrm{I}}^{\mathrm{aux}} = K_{\mathrm{III}}^{\mathrm{aux}} = 0$ and $K_{\mathrm{III}}^{\mathrm{aux}} = 1$, $K_{\mathrm{I}}^{\mathrm{aux}} = K_{\mathrm{II}}^{\mathrm{aux}} = 0$, respectively.

2.3. Domain form of the interaction integral

Since the domain expression is naturally compatible with the finite element formulation of the field equations (Shih et al., 1986), the domain representation of the interaction integral in Eq. (4) is derived in this section. To begin, consider a small segment L_c on a curved crack front around the point s as shown in Fig. 2(a) and at a point p on it, the virtual crack advance is assumed

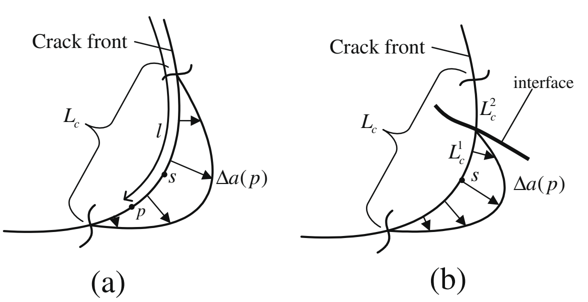

Fig. 2. Virtual crack advance at the segment L_c on the crack front.

$$\delta\xi_l = c_l(p)\Delta a(p) \tag{7}$$

where $\Delta a(p)$ is the magnitude of the crack advance. It is assumed that $\Delta a(p)$ only varies continuously along the segment L_c and is zero at any point outside L_c. The total energy caused by the interaction integral $I(p)$ due to the crack advance $\delta\xi_l$ on the segment L_c is defined as

$$\bar{I} = \int_{L_c} I(p)\Delta a(p) \, dl \tag{8}$$

Since the segment L_c is very small, it can be assumed that the interaction integral $I(p)$ varies slowly along the segment L_c. With this assumption, $I(p)$ in Eq. (8) can be replaced by a constant $I(s)$ and thus, $I(s)$ can be obtained by the relation

$$I(s) = \frac{\bar{I}}{\int_{L_c} \Delta a(p) \, dl} \tag{9}$$

Therefore, the integral $\bar{I}$ should be solved firstly. As shown in Fig. 3, since the crack faces are assumed to be traction-free, it can be easily proved that (Kim and Paulino, 2003)

$$I(p) = -\lim_{\Gamma\to 0} \oint_{\Gamma_0} P_{lj} m_j c_l(p) \bar{q} \, d\Gamma \tag{10}$$

Here, $\Gamma_0 = \Gamma_B + \Gamma_c^+ + \Gamma^- + \Gamma_c^-$ is a contour in ξ_1–ξ_2-plane (the definitions of the curvilinear coordinates ξ_1, ξ_2 and ξ_3 are given in Appendix A), where Γ^- is the opposite integral path of Γ, m_i is the unit outward normal vector to the contour Γ_0 and therefore, $m_i = -n_i$ on Γ, $\bar{q}$ is an arbitrary function with values varying smoothly from 1 on Γ to 0 on Γ_B.

The area enclosed by Γ_0 is denoted by the symbol A_0. By sweeping the area A_0 on L_c and keeping them in ξ_1–ξ_2-plane, we can get a tubular volume V_0 enclosed by the surface S_0 as shown in Fig. 3. The closed surface S_0 consists of four curved surfaces S, S_c^+, S_c^- and S_B generated by sweeping Γ^-, Γ_c^+, Γ_c^- and Γ_B on L_c, respectively, and two planar surfaces S_1 and S_2. By substituting Eq. (10) into Eq. (8), $\bar{I}$ can be expressed as a surface integral as follows:

$$\bar{I} = -\lim_{S\to 0} \oint_{S_0} P_{lj} m_j q_l \, dS, \quad q_l = c_l \bar{q} \Delta a \tag{11}$$

Here, q_l is a smooth test function with values varying from $c_l\Delta a$ on S to 0 on S_B.

Taking the limit $S \to 0$ leads to $V_0 \to V$. When the material properties in the volume V vary continuously, applying divergence theorem to Eq. (11), we have

$$\bar{I} = -\int_V \left(P_{lj} q_{l,j} + P_{lj,j} q_l\right) dV \tag{12}$$

Substituting P_{lj} given in Eq. (5) into Eq. (12), one obtains

$$\bar{I} = \int_V \left(u_{i,l}\sigma_{ij}^{\mathrm{aux}} q_{l,j} + u_{i,l}^{\mathrm{aux}}\sigma_{ij} q_{l,j} - \sigma_{ik}^{\mathrm{aux}}\varepsilon_{ik} q_{l,l}\right) dV + \int_V \left(u_{i,lj}\sigma_{ij}^{\mathrm{aux}} + u_{i,l}\sigma_{ij,j}^{\mathrm{aux}} + u_{i,lj}^{\mathrm{aux}}\sigma_{ij} + u_{i,l}^{\mathrm{aux}}\sigma_{ij,j} - \sigma_{ij,l}^{\mathrm{aux}}\varepsilon_{ij} - \sigma_{ij}^{\mathrm{aux}}\varepsilon_{ij,l}\right) q_l \, dV \tag{13}$$

Here, the symmetry of the auxiliary stress tensor leads to $\sigma_{ij}^{\mathrm{aux}} u_{i,lj} - \sigma_{ij}^{\mathrm{aux}}\varepsilon_{ij,l} = 0$. And according to the equilibrium of the actual stresses with a known body force f_i, i.e., $\sigma_{ij,j} + f_i = 0$, $\bar{I}$ can be simplified as

$$\bar{I} = \int_V \left(u_{i,l}\sigma_{ij}^{\mathrm{aux}} q_{l,j} + u_{i,l}^{\mathrm{aux}}\sigma_{ij} q_{l,j} - \sigma_{ij}^{\mathrm{aux}}\varepsilon_{ij} q_{l,l}\right) dV + \int_V \left(u_{i,l}\sigma_{ij,j}^{\mathrm{aux}} + u_{i,lj}^{\mathrm{aux}}\sigma_{ij} - u_{i,l}^{\mathrm{aux}} f_i - \sigma_{ij,l}^{\mathrm{aux}}\varepsilon_{ij}\right) q_l \, dV \tag{14}$$

Whether the material properties are homogeneous or nonhomogeneous, the second term in Eq. (14) is not zero (Nahta and Moran, 1993; Gosz et al., 1998; Walters et al., 2006).

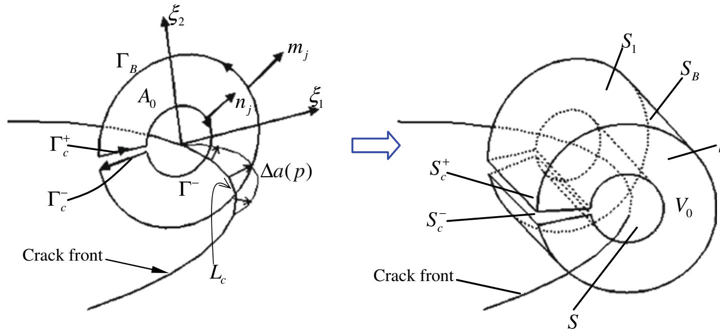

Fig. 3. A closed integral on the surface perpendicular to the crack front and its equivalent volume integral in a tubular domain.

Since the segment L_c is very small, the material properties are assumed to vary slowly on it and therefore, the material properties at point s are used in the definitions of the auxiliary stresses and displacements for any point in the integral volume V. As a result of the above analysis, it is interesting to find that compared with the integral $\bar{I}$ given by Walters et al. (2005, 2006) for nonhomogeneous materials, the expression in Eq. (14) does not contain any derivatives of the material properties. Therefore, the interaction integral does not need the material properties to be differentiable. Since it may be difficult to obtain the derivatives of material properties or there are no derivatives in many actual cases, the applicable range of the present interaction integral is wider than that of the traditional J-integral for nonhomogeneous materials.

3. Influence of the interfaces (material discontinuities) on the interaction integral

In the above section, it is shown that the interaction integral method does not need the nonhomogeneous material properties to be differentiable. However, the material properties are still required to be continuous in the above derivation. In this section, we will discuss whether the continuity condition of material properties is necessary in the interaction integral method.

3.1. Domain form of the interaction integral for discontinuous materials

As shown in Fig. 4(a), the integral domain V is divided by a material interface $S_{\text{interface}}$ into two domains V_1 and V_2. In each domain, the material properties vary continuously. And the closed surface S_0 defined in the above section is cut into two unclosed surfaces S_{01} and S_{02}. The integral in Eq. (11) can be rewritten as

$$\bar{I} = -\lim_{S\to 0} \oint_{S_{01}+S_{\text{interface}}} P_{lj} m_j q_l \, dS - \oint_{S_{02}+S^-_{\text{interface}}} P_{lj} m_j q_l \, dS + I^*_{\text{interface}} \tag{15}$$

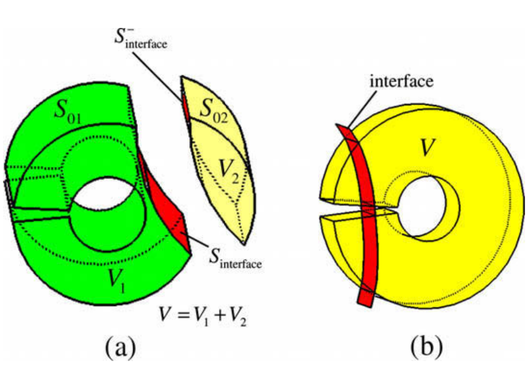

Fig. 4. The tubular integral domain cut by an arbitrarily curved interface.

where $I^*_{\text{interface}}$ is a surface integral along the interface with the expression shown below

$$I^*_{\text{interface}} = \int_{S_{\text{interface}}} (P_{lj} m_j q_l)^{①} \, dS + \int_{S^-_{\text{interface}}} (P_{lj} m_j q_l)^{②} \, dS \tag{16}$$

Here, the variables or expressions on the interface marked by the superscripts ① and ② means that they belong to the domains V_1 and V_2, respectively.

According to the definitions of auxiliary fields in Appendix A, it can be observed that the auxiliary stresses and displacements and their derivatives are continuous on the interface. Therefore, $\left(\sigma_{ij}^{\text{aux}}\right)^{①} = \left(\sigma_{ij}^{\text{aux}}\right)^{②} = \sigma_{ij}^{\text{aux}}$ and $\left(u_{i,l}^{\text{aux}}\right)^{①} = \left(u_{i,l}^{\text{aux}}\right)^{②} = u_{i,l}^{\text{aux}}$. Since the interface $S^-_{\text{interface}}$ is the opposite surface of $S_{\text{interface}}$ and according to the definition of P_{lj} in Eq. (5), $I^*_{\text{interface}}$ can be rewritten as

$$\begin{aligned} I^*_{\text{interface}} = \int_{S_{\text{interface}}} \Big[& \sigma_{ij}^{\text{aux}} \left(\varepsilon_{ij}^{①} - \varepsilon_{ij}^{②}\right) m_l q_l - \left(\sigma_{ij}^{①} - \sigma_{ij}^{②}\right) u_{i,l}^{\text{aux}} m_j q_l \\ & - \sigma_{ij}^{\text{aux}} \left(u_{i,l}^{①} - u_{i,l}^{②}\right) m_j q_l \Big] dS \end{aligned} \tag{17}$$

The value of $I^*_{\text{interface}}$ will be given in the following part. By applying divergence theorem to the first and second integrals in Eq. (15), respectively, we have

$$\bar{I} = -\int_{V_1} (P_{lj} q_{l,j} + P_{lj,j} q_l) \, dV - \int_{V_2} (P_{lj} q_{l,j} + P_{lj,j} q_l) \, dV + I^*_{\text{interface}} \tag{18}$$

3.2. Interface integral $I^*_{\text{interface}}$

Without loss of generality, an arbitrarily curved material interface $S_{\text{interface}}$ is shown in Fig. 5 and its mathematical description can be written as

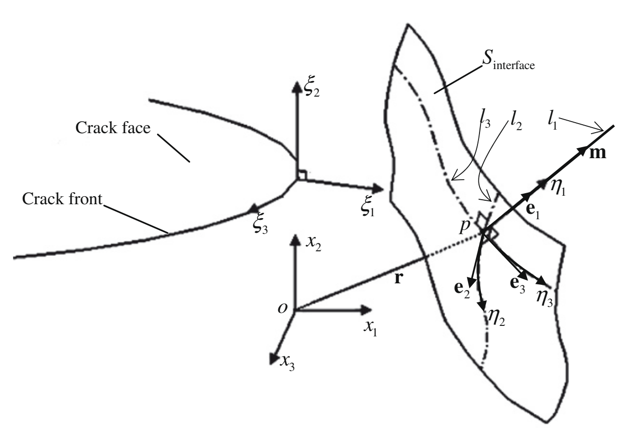

Fig. 5. An arbitrarily curved interface and an orthogonal curvilinear coordinate system associated with it.

$$f(x_1, x_2, x_3) = 0 \tag{19}$$

At a point p on the interface, an orthogonal curvilinear coordinate system is defined. The vector $\mathbf{m}$ is the unit outward normal vector to the surface $S_{\text{interface}}$ at point p. The straight line where the vector $\mathbf{m}$ lies is denoted by the symbol l_1. We select two mutually perpendicular planes containing the line l_1 and let the symbols l_2 and l_3 denote the curves generated by the intersection of the surface $S_{\text{interface}}$ and the two planes. Then, three orthotropic curvilinear coordinates η_1, η_2 and η_3 are defined on the lines l_1, l_2 and l_3, respectively. Here, η_1 gives the signed distance of a point to the surface $S_{\text{interface}}$. The natural base vectors $\mathbf{h}_i$ corresponding to the coordinates are defined by

$$\mathbf{h}_i = \frac{\partial x_k}{\partial \eta_i}\mathbf{i}_k \tag{20}$$

where x_k are the Cartesian coordinates and $\mathbf{i}_k$ are the corresponding base vectors. For convenience, we define the orthogonal unit base vectors $\mathbf{e}_i$ by

$$\mathbf{e}_i = \frac{\mathbf{h}_i}{A_{\underline{i}}} \tag{21}$$

where $A_i = \sqrt{\mathbf{h}_{\underline{i}} \cdot \mathbf{h}_{\underline{i}}}$ and the underlined subscript i denotes no sum on i. It is obvious from the above definitions that $\mathbf{e}_1 = \mathbf{m}$ and the scale factor $A_1 = 1$ (Gosz and Moran, 2002). In this subsection, the variables or expressions marked by the subscripts i, j, k and l denote their components in (η_1, η_2, η_3) coordinate system.

The integral $I^*_{\text{interface}}$ in Eq. (17) can be rewritten in tensor form as

$$I^*_{\text{interface}} = \int_{S_{\text{interface}}} \left\{ \boldsymbol{\sigma}^{\text{aux}} : (\boldsymbol{\varepsilon}^{①} - \boldsymbol{\varepsilon}^{②})\mathbf{q}\cdot\mathbf{m} - \mathbf{m}\cdot\left(\boldsymbol{\sigma}^{①} - \boldsymbol{\sigma}^{②}\right)\cdot(\mathbf{u}^{\text{aux}}\nabla) \cdot\mathbf{q} - \mathbf{m}\cdot\boldsymbol{\sigma}^{\text{aux}}\cdot\left[(\mathbf{u}\nabla)^{①} - (\mathbf{u}\nabla)^{②}\right]\cdot\mathbf{q}\right\} dS \tag{22}$$

where ∇ is the gradient operator expressed by (Gosz and Moran, 2002)

$$\nabla = \left\{ \mathbf{e}_1 \frac{1}{A_1}\frac{\partial}{\partial\eta_1} + \mathbf{e}_2 \frac{1}{A_2}\frac{\partial}{\partial\eta_2} + \mathbf{e}_3 \frac{1}{A_3}\frac{\partial}{\partial\eta_3} \right\} \tag{23}$$

According to the equilibrium condition on the bimaterial interface, the tractions on both sides of the interface should be equal. That is

$$\mathbf{m}\cdot\boldsymbol{\sigma}^{①} = \mathbf{m}\cdot\boldsymbol{\sigma}^{②} \tag{24}$$

Since the interface is perfectly bonded, the derivatives of actual displacements with respect to the curvilinear coordinates η_2 and η_3 are equal on both sides of the interface, i.e.,

$$\left(\frac{\partial\mathbf{u}}{\partial\eta_2}\right)^{①} = \left(\frac{\partial\mathbf{u}}{\partial\eta_2}\right)^{②}, \quad \left(\frac{\partial\mathbf{u}}{\partial\eta_3}\right)^{①} = \left(\frac{\partial\mathbf{u}}{\partial\eta_3}\right)^{②} \tag{25}$$

Since the stress $\boldsymbol{\sigma}^{\text{aux}}$ is a symmetrical tensor, by applying the strain–displacement relations of actual fields, the first integrand in Eq. (22) can be written as

$$\boldsymbol{\sigma}^{\text{aux}} : (\boldsymbol{\varepsilon}^{①} - \boldsymbol{\varepsilon}^{②})\mathbf{q}\cdot\mathbf{m} = \boldsymbol{\sigma}^{\text{aux}} : \left[(\nabla\mathbf{u})^{①} - (\nabla\mathbf{u})^{②}\right]\mathbf{q}\cdot\mathbf{m} \tag{26}$$

In (η_1, η_2, η_3) coordinate system, $m_1 = 1$ and $m_2 = m_3 = 0$. Therefore, $\mathbf{q}\cdot\mathbf{m} = q_1$ and Eq. (26) can be written as

$$\boldsymbol{\sigma}^{\text{aux}} : (\boldsymbol{\varepsilon}^{①} - \boldsymbol{\varepsilon}^{②})\mathbf{q}\cdot\mathbf{m} = \sigma^{\text{aux}}_{lj}\mathbf{e}_j \cdot \frac{1}{A_{\underline{l}}}\left[\left(\frac{\partial\mathbf{u}}{\partial\eta_l}\right)^{①} - \left(\frac{\partial\mathbf{u}}{\partial\eta_l}\right)^{②}\right] q_1 \tag{27}$$

The detailed derivations of Eq. (27) are given in Appendix B. Substituting Eq. (25) and $A_1 = 1$ into Eq. (27), we have

$$\boldsymbol{\sigma}^{\text{aux}} : (\boldsymbol{\varepsilon}^{①} - \boldsymbol{\varepsilon}^{②})\mathbf{q}\cdot\mathbf{m} = \sigma^{\text{aux}}_{1j}\mathbf{e}_j \cdot \left[\left(\frac{\partial\mathbf{u}}{\partial\eta_1}\right)^{①} - \left(\frac{\partial\mathbf{u}}{\partial\eta_1}\right)^{②}\right] q_1 \tag{28}$$

According to Eq. (24), the second integrand in Eq. (22) is

$$\mathbf{m}\cdot\left(\boldsymbol{\sigma}^{①} - \boldsymbol{\sigma}^{②}\right)\cdot(\mathbf{u}^{\text{aux}}\nabla)\cdot\mathbf{q} = 0 \tag{29}$$

The third integrand in Eq. (22) can be written as

$$\mathbf{m}\cdot\boldsymbol{\sigma}^{\text{aux}}\cdot\left[(\mathbf{u}\nabla)^{①} - (\mathbf{u}\nabla)^{②}\right]\cdot\mathbf{q} = m_i\sigma^{\text{aux}}_{ij}\mathbf{e}_j \cdot \frac{1}{A_{\underline{l}}}\left[\left(\frac{\partial\mathbf{u}}{\partial\eta_l}\right)^{①} - \left(\frac{\partial\mathbf{u}}{\partial\eta_l}\right)^{②}\right] q_l \tag{30}$$

Substituting $A_1 = 1$, $m_1 = 1$, $m_2 = m_3 = 0$ and Eq. (25) into Eq. (30), one obtains

$$\mathbf{m}\cdot\boldsymbol{\sigma}^{\text{aux}}\cdot\left[(\mathbf{u}\nabla)^{①} - (\mathbf{u}\nabla)^{②}\right]\cdot\mathbf{q} = \sigma^{\text{aux}}_{1j}\mathbf{e}_j \cdot \left[\left(\frac{\partial\mathbf{u}}{\partial\eta_1}\right)^{①} - \left(\frac{\partial\mathbf{u}}{\partial\eta_1}\right)^{②}\right] q_1 \tag{31}$$

Substituting Eqs. (28), (29) and (31) into Eq. (22) yields

$$I^*_{\text{interface}} = 0 \tag{32}$$

Similarly, the same result can be obtained for the interface which passes through the crack faces as shown in Fig. 4(b). If the interface intersects with the crack front in the segment L_c which is cut into two parts L_c^1 and L_c^2 as shown in Fig. 2(b), the crack advance $\Delta a(p)$ only varies on L_c^1 which contains the point s and remains zero on L_c^2. Actually, the above treatment means that the segment L_c is replaced by L_c^1.

3.3. Discussion on the interaction integral

Substituting Eq. (32) and P_{lj} given in Eq. (5) into Eq. (18), the same expression as Eq. (14) is obtained. It implies that Eq. (14) is still valid for nonhomogeneous materials with material interfaces in the integral domain. By substituting Eq. (14) into Eq. (9), the interaction integral is obtained as

$$I(s) = \frac{\int_V \left[\left(u_{i,l}\sigma^{\text{aux}}_{ij}q_{l,j} + u^{\text{aux}}_{i,l}\sigma_{ij}q_{l,j} - \sigma^{\text{aux}}_{ij}\varepsilon_{ij}q_{l,l}\right) + \left(u_{i,l}\sigma^{\text{aux}}_{ij,j} + u^{\text{aux}}_{i,lj}\sigma_{ij} - f_i u^{\text{aux}}_{i,l} - \sigma^{\text{aux}}_{ij,l}\varepsilon_{ij}\right)q_l\right] dV}{\int_{L_c}\Delta a(p)\,dl} \tag{33}$$

For the numerical examples in this paper, no body force is assumed (i.e., $f_i = 0$) and the finite element discretization of Eq. (33) without body force is given in Appendix C.

The interaction integral in Eq. (33) does not require the material properties to be continuous and hence, its applicable range is greatly enlarged. Moreover, the expression in Eq. (33) can facilitate the numerical implementation for the materials with complicated material interfaces around the crack tip since the integral domain can be chosen arbitrarily.

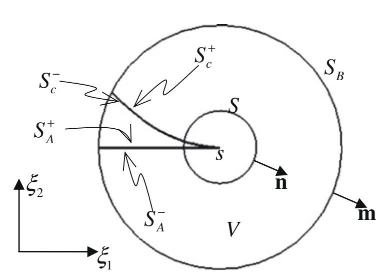

Fig. 6. Cross-section of a tubular integral domain around the segment L_c on the crack front.

If the crack faces in the integral domain V are curved as shown in Fig. 6, the interaction integral is

$$I(s) = \frac{\int_V \left[\left(u_{i,l}\sigma_{ij}^{\text{aux}}q_{l,j} + u_{i,l}^{\text{aux}}\sigma_{ij}q_{l,j} - \sigma_{ij}^{\text{aux}}\varepsilon_{ij}q_{l,l}\right) + \left(u_{i,l}\sigma_{ij,j}^{\text{aux}} + u_{i,lj}^{\text{aux}}\sigma_{ij} - f_i u_{i,l}^{\text{aux}} - \sigma_{ij,l}^{\text{aux}}\varepsilon_{ij}\right)q_l\right]dV + I_{\text{crackface}}}{\int_{L_c}\Delta a(p)\,dl} \tag{34}$$

where $I_{\text{crackface}}$ is a surface integral on the crack faces. According to Gosz and Moran (2002), the surface integral $I_{\text{crackface}}$ is

$$I_{\text{crackface}} = \int_{S_c^+ + S_c^- + S_A^+ + S_A^-} P_{lj}m_j q_l \, dS \tag{35}$$

where S_A^+ is a fictitious crack face tangent to the crack front and S_A^- is its opposite surface. Since the auxiliary displacement components and certain auxiliary stress and strain components are discontinuous across the surfaces S_A^+ and S_A^-, the surface integral on S_A^+ and S_A^- of $I_{\text{crackface}}$ appears.

4. Numerical examples and discussions

In order to demonstrate the accuracy of the interaction integral method and verify the convergence of the method, we will present several numerical examples on the 3D fracture problems for the materials with continuous nonhomogeneous properties and discontinuous properties, respectively.

4.1. Example 1: functionally graded plate with a semi-elliptical surface crack

Fig. 7(a) shows a 3D functionally graded plate of length $2L$, width $2h$ and thickness t under tension load. The plate contains a semi-elliptical surface crack of half-length c and depth a. The problem of a plate with such a configuration was investigated by Walters et al. (2004). In order to simulate infinite plate, both the length $2L$ and the width $2h$ of the plate remain fixed at 10 times of the thickness t. The tension load σ_0 is applied along the top and the bottom edges of the plate. The Young's modulus E varies only in the thickness (x_1) direction from $E_1 = E(x_1 = 0)$ to $E_2 = E(x_1 = t)$ and the Poisson's ratio ν is constant. The following data and expressions are used for numerical analysis: $L = h = 1000$; $t/h = 0.2$; $a/t = 0.5$; $a/c = 1$; $E(x_1) = E_1 e^{\beta x_1}$; $\beta = \frac{1}{t}\ln(E_2/E_1)$; $E_2/E_1 = (0.2, 1, 5)$; $\nu = 0.25$; $\sigma_0 = 1$. The SIFs are normalized by $K_0 = \sigma_0\sqrt{\pi a/Q}$, where $Q = 1 + 1.464(a/c)^{1.65}$ for $a/c \leqslant 1$ and $Q = 1 + 1.464(c/a)^{1.65}$ for $a/c > 1$ (Walters et al., 2004).

Symmetry permits modeling of only one half plate and Fig. 7(b) and (c) shows the mesh configuration. Twenty-node hexahedral elements are used over most of the mesh and sixteen 20-node, quarter-point, hexagonal elements with collapsed faces surrounding each crack front as shown in Fig. 8(a). The crack front is divided into 16 elements in ξ_3 direction from $\phi = 0$ to $\phi = \pi/2$, where the angle ϕ is shown in Fig. 7(a). The mesh consists of 10,848 hexahedral and 256 hexagonal elements, with a total of 11,104 elements

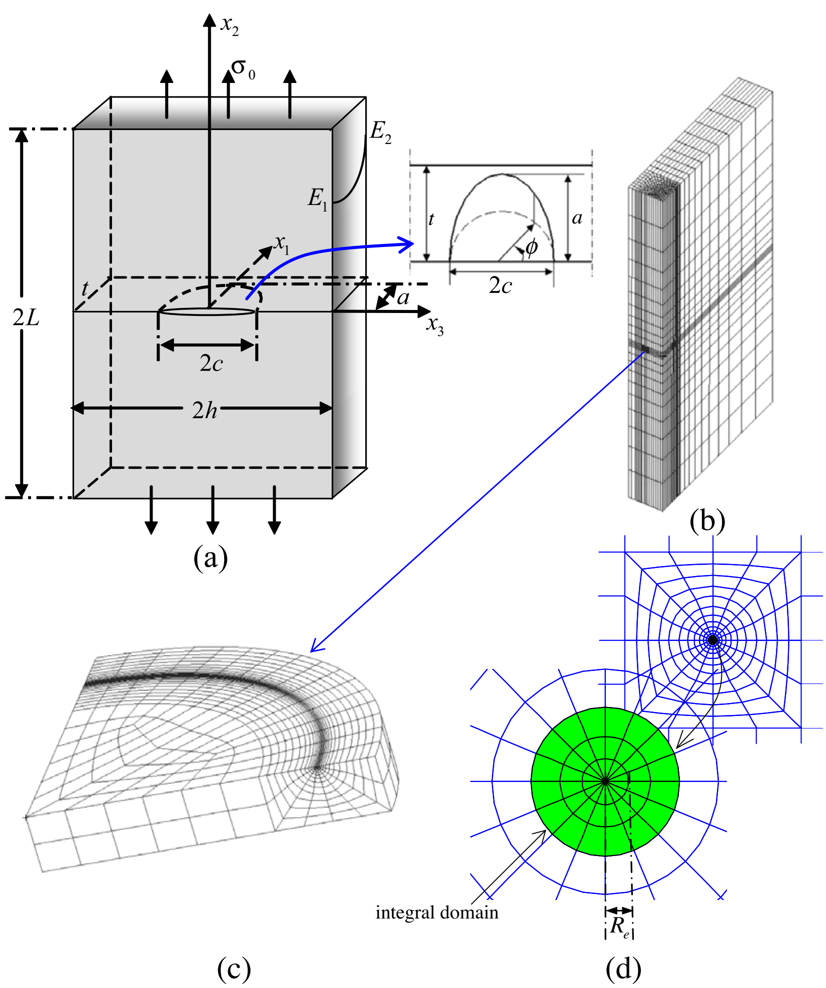

Fig. 7. A functionally graded plate with a semi-elliptical surface crack: (a) geometry and boundary conditions; (b) finite element mesh; (c) mesh around the crack front; and (d) cross-section of the integral domain.

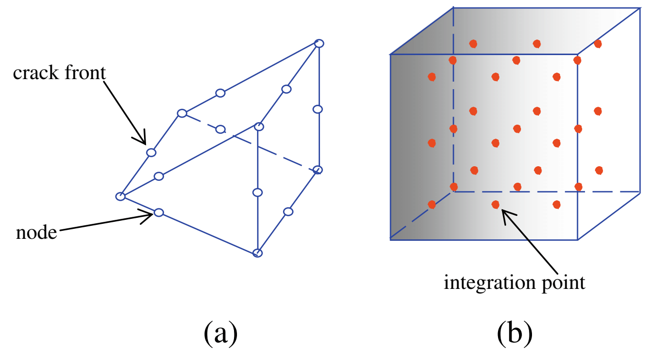

Fig. 8. Schematic of finite elements and integration points: (a) a 20-node, quarter-point, hexagonal element; (b) a 20-node hexahedral element with integration points for nonhomogeneous materials.

and 49,156 nodes. In order to improve numerical precision, the ratio of the radial edge length R_e of the elements at the crack front to the crack depth a is $R_e/a = 0.003$. In this subsection, three-layer elements around the crack tip are adopted for the calculation of the interaction integral as shown in Fig. 7(d). Since material properties are nonhomogeneous, as shown in Fig. 8(b), actual material properties at integration points are adopted when the element stiffness matrix is formed (Yu et al., 2007). For all examples in this paper, we use $3 \times 3 \times 3$ Gauss quadrature in FEM computation and $2 \times 2 \times 2$ Gauss quadrature in the calculation of the interaction integral. The comparison between the normalized SIFs computed by Eq. (33) and the results in Walters et al. (2004) is shown in Table 1. The geometry, loading and material property variations lead to mode-I conditions on the crack plane and thus, only mode-I normalized SIFs K_I/K_0 are listed along the crack front from the angle $\phi = 0$ to $\phi = \pi/2$. It can be found that the relative errors of the mode-I normalized SIFs are all within 0.6% for homogeneous materials and 2% for FGMs. Excellent agreement demonstrates that the present method is valid for the fracture problem of nonhomogeneous materials with continuous properties.

It should be pointed out that near the free surface, the stress singularity ($r^{-\lambda}$) becomes weaker ($\lambda < 1/2$) and the mode-I SIF tends toward zero at $\phi = 0$ (Pook, 1994). Nakamura and Parks (1988) gave the estimation of the influence region of free surface on the singularity in semi-elliptical surface cracks nearly to be $0.03a^2/c$. Since the present study does not focus on the region near free surface, the mesh near free surface is not refined and 2D plane-strain asymptotic solution (Kim et al., 2001) are chosen to be the auxiliary fields to solve the SIFs at all points.

Subsequently, we select seven cylindrical integral domains with different radial sizes to verify the domain-independence of the interaction integral. In order to select the integral domains, we define R_I to be the radius of the referenced cylindrical surface C_I by which the integral domain is determined as shown in Fig. 9. In details, the integral domain consists of the elements cut by C_I and the elements surrounded by C_I. Table 2 lists the mode-I normalized SIFs along the crack front for the ratio $R_I/R_e = (3,6,12,24,36,48,60)$. In order to estimate the dispersion of interaction integral, the relative error is defined as

Table 1
Normalized SIFs K_I/K_0 along the crack front in FGM plate under tension (Example 1: $a/t = 0.5$; $a/c = 1$; $E(x_1) = E_1 e^{\beta x_1}$; $\beta = \frac{1}{t}\ln(E_2/E_1)$; $\nu = 0.25$; $K_0 = \sigma_0\sqrt{\pi a/Q}$).

$\frac{2\phi}{\pi}$	Present results E_2/E_1			Walters et al. (2004) E_2/E_1			Relative errors (%) E_2/E_1		
	0.2	1.0	5.0	0.2	1.0	5.0	0.2	1.0	5.0
0.000	1.346	1.243	0.903	1.351	1.240	0.907	−0.37	0.24	−0.44
0.125	1.248	1.210	0.973	1.238	1.209	0.965	0.80	0.08	0.82
0.250	1.170	1.155	1.027	1.161	1.155	1.019	0.77	0.00	0.78
0.375	1.121	1.122	1.083	1.109	1.124	1.075	1.07	−0.18	0.74
0.500	1.084	1.101	1.134	1.071	1.101	1.125	1.20	0.00	0.79
0.625	1.055	1.088	1.177	1.041	1.087	1.166	1.33	0.09	0.93
0.750	1.033	1.080	1.208	1.019	1.078	1.197	1.35	0.18	0.91
0.875	1.020	1.074	1.226	1.004	1.070	1.212	1.57	0.37	1.14
1.000	1.016	1.073	1.232	0.997	1.067	1.213	1.87	0.56	1.54

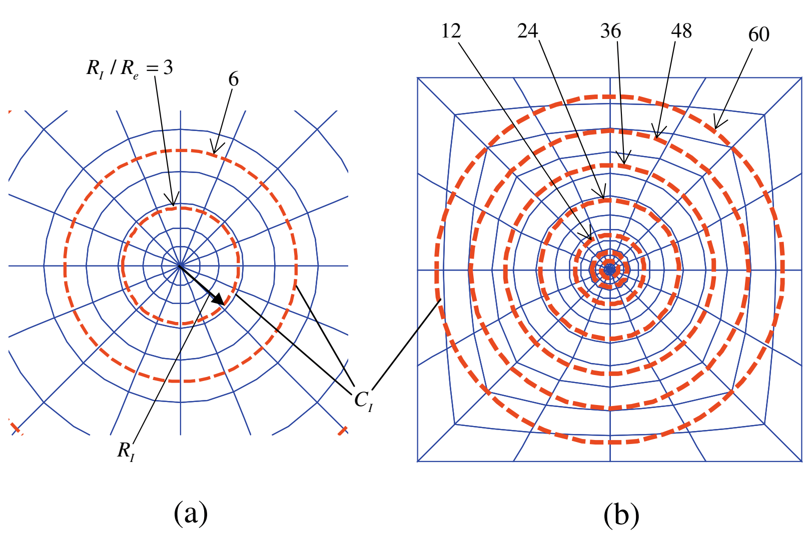

Fig. 9. Cross-section of seven integral domains.

Table 2
Normalized SIFs K_I/K_0 along the crack front for different integral domains (Example 1: $a/t = 0.5$; $a/c = 1$; $E(x_1) = E_1 e^{\beta x_1}$; $\beta = \frac{1}{t}\ln(E_2/E_1)$; $\nu = 0.25$; $K_0 = \sigma_0\sqrt{\pi a/Q}$).

$\frac{E_2}{E_1}$	$\frac{2\phi}{\pi}$	R_I/R_e							Mean	E_{rr} (%)
		3	6	12	24	36	48	60		
1.0	0.125	1.2113	1.2109	1.2112	1.2115	1.2119	1.2119	1.2121	1.2115	0.10
	0.250	1.1567	1.1561	1.1567	1.1569	1.1571	1.1570	1.1573	1.1568	0.10
	0.375	1.1241	1.1236	1.1241	1.1243	1.1245	1.1244	1.1246	1.1242	0.09
	0.500	1.1031	1.1025	1.1030	1.1032	1.1034	1.1033	1.1035	1.1031	0.09
	0.625	1.0898	1.0893	1.0898	1.0899	1.0901	1.0900	1.0902	1.0899	0.08
	0.750	1.0815	1.0809	1.0814	1.0816	1.0818	1.0817	1.0819	1.0815	0.09
	0.875	1.0763	1.0758	1.0763	1.0764	1.0766	1.0765	1.0767	1.0764	0.08
	1.000	1.0748	1.0743	1.0748	1.0749	1.0751	1.0750	1.0752	1.0749	0.08
0.2	0.125	1.2480	1.2491	1.2495	1.2499	1.2502	1.2502	1.2505	1.2496	0.20
	0.250	1.1702	1.1714	1.1720	1.1722	1.1725	1.1724	1.1727	1.1719	0.21
	0.375	1.1211	1.1223	1.1228	1.1230	1.1233	1.1233	1.1235	1.1228	0.21
	0.500	1.0839	1.0851	1.0856	1.0858	1.0861	1.0861	1.0864	1.0856	0.23
	0.625	1.0551	1.0562	1.0567	1.0570	1.0572	1.0573	1.0575	1.0567	0.23
	0.750	1.0336	1.0348	1.0353	1.0356	1.0358	1.0359	1.0361	1.0353	0.24
	0.875	1.0201	1.0212	1.0218	1.0220	1.0223	1.0223	1.0226	1.0218	0.24
	1.000	1.0160	1.0170	1.0175	1.0177	1.0180	1.0180	1.0183	1.0175	0.23

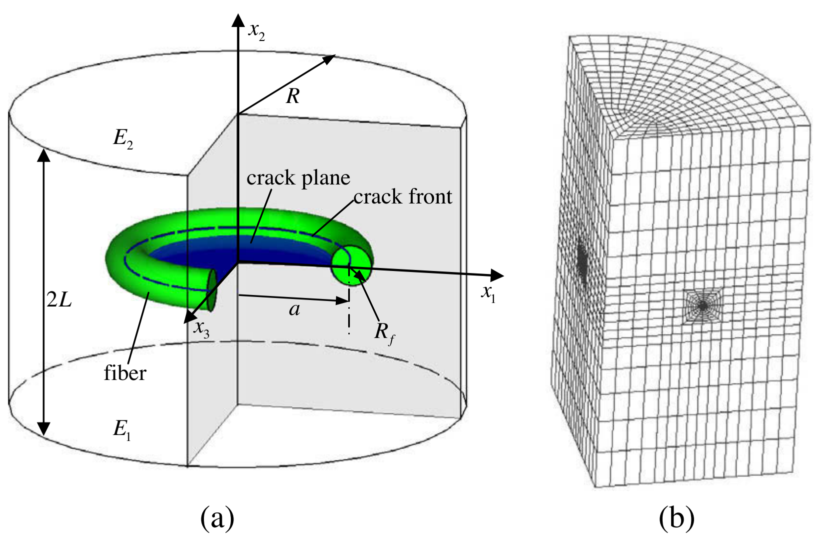

Fig. 10. An annular-fiber-reinforced cylinder with a penny-shaped crack: (a) geometry and boundary conditions; (b) finite element mesh.

$$E_{rr} = \left|\frac{K_{\max} - K_{\min}}{K_{\mathrm{mean}}}\right| \times 100\% \tag{36}$$

where $K_{\max}$, $K_{\min}$ and K_{mean} denote the maximum, minimum and mean of the SIFs, respectively, at a point s. The results show that the relative errors (E_{rr}) of the mode-I normalized SIFs for every point on the crack front are all within 0.10% for $E_2/E_1 = 1$ and within 0.25% for $E_2/E_1 = 0.2$. It implies that the interaction integral in Eq. (33) is domain-independent for a 3D curved crack in the material with the properties varying continuously.

4.2. Example 2: domain-independence for the materials with interfaces

In order to check the influence of the interface on the interaction integral, we investigate an annular-fiber-reinforced cylinder with a penny-shaped crack under uniform tension σ_0 as shown in Fig. 10(a). The cylinder has a radius R and total length $2L$. The crack of radius a is located in the center of the cylinder and the crack front coincides with the midline of the fiber which has a radius R_f. In the cylinder, the Young's modulus $E(x_2)$ varies only in the length (x_2) direction from E_1 at the bottom surface to E_2 at the top surface and the Poisson's ratio ν is constant. For the fiber, the

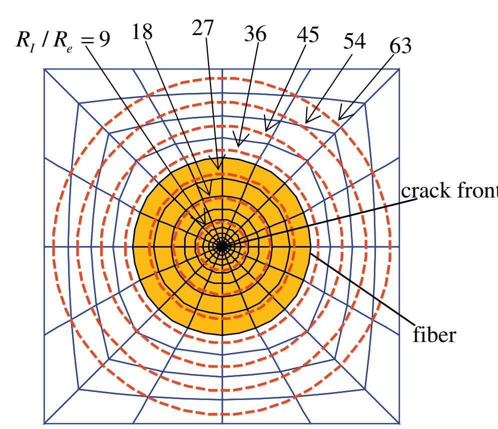

Fig. 11. Cross-section of seven integral domains around the crack front in the fiber-reinforced cylinder.

Young's modulus E_f and the Poisson's ratio ν are both constant. The following data and expressions are used for numerical analysis: $L = R = 200$; $a = 100$; $R_f = 10$; $E(x_2) = E_1 e^{\beta(x_2 + L)}$; $\beta = \frac{1}{2L}\ln(E_2/E_1)$;

Table 3
Normalized SIFs of a penny-shaped crack in a fiber-reinforced cylinder under uniform tension (Example 2: $R = L = 200$; $a = 100$; $R_f = 10$; $K_0 = \sigma_0\sqrt{\pi a/Q}$).

$\frac{E_2}{E_1}$	$\frac{E_f}{E_1}$	SIFs	R_I/R_e							Mean	E_{rr} (%)
			9	18	27	36	45	54	63		
1	10	K_I/K_0	3.2565	3.2558	3.2546	3.2535	3.2520	3.2534	3.2527	3.2541	0.14
	100	K_I/K_0	4.9869	4.9849	4.9826	4.9748	4.9638	4.9698	4.9645	4.9753	0.46
10	100	K_I/K_0	4.3294	4.3282	4.3265	4.3237	4.3197	4.3231	4.3234	4.3248	0.22
		K_{II}/K_0	0.1322	0.1310	0.1296	0.1292	0.1314	0.1296	0.1317	0.1308	2.29
100	100	K_I/K_0	2.9528	2.9526	2.9520	2.9511	2.9500	2.9513	2.9517	2.9517	0.10
		K_{II}/K_0	0.2899	0.2886	0.2870	0.2862	0.2872	0.2869	0.2895	0.2879	1.04

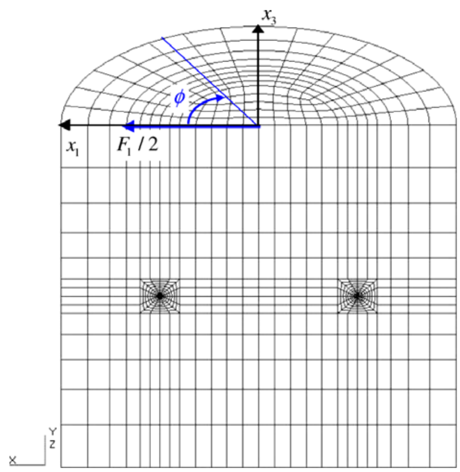

Fig. 12. Finite element mesh configuration of one half of the cylinder.

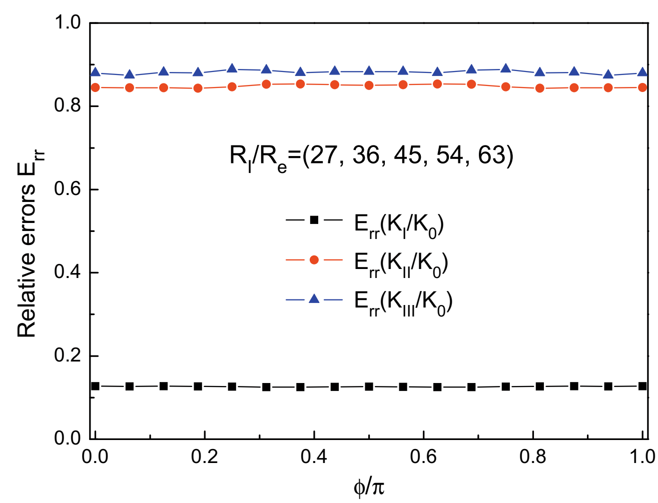

Fig. 14. Relative errors E_{rr} of the mixed-mode SIFs obtained in different integral domains along the crack front in a cylinder under a centralized force.

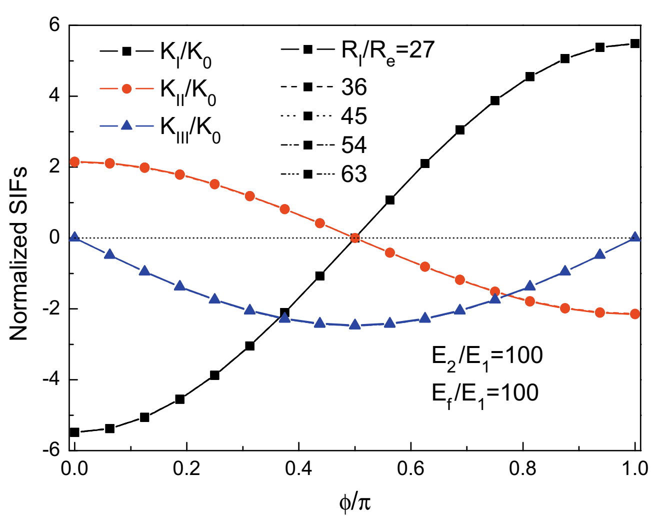

Fig. 13. Normalized SIFs along crack front in a cylinder under a centralized force.

$E_2/E_1 = (1, 10, 100)$; $E_f/E_1 = 100$; $\nu = 0.25$; $\sigma_0 = 1$; $K_0 = \sigma_0\sqrt{\pi a/Q}$; $Q = 2.464$.

Fig. 10(b) shows the mesh configuration corresponding to a quarter of the cylinder. The mesh consists of 7612 elements and 33,715 nodes. The ratio of the radial edge length R_e of the elements at the crack front to the crack radius a is $R_e/a = 0.003$. Seven different integral domains ($R_I/R_e = 9, 18, 27, 36, 45, 54, 63$) are selected to test the stability of the numerical results and the latter four domains contain the interface as shown in Fig. 11.

Table 3 lists the mixed-mode normalized SIFs for the cases of homogeneous and nonhomogeneous matrix materials. Only mode-I normalized SIFs for $E_2/E_1 = 1$ are listed since the symmetry leads to pure mode-I conditions. The results show that the relative errors (E_{rr}) defined in Eq. (36) are all within 0.46% for K_I/K_0 and within 2.29% for K_{II}/K_0. Compared with K_I/K_0, the values of K_{II}/K_0 are very small for $E_2/E_1 = 10$ and $E_2/E_1 = 100$. Although the relative errors of K_{II}/K_0 are a little large, the absolute errors of K_{II}/K_0 is not larger than those of K_I/K_0. In order to show the influences of the integral domains on the SIFs of different modes better, a new example with the mode-I, mode-II and mode-III SIFs of the same magnitude will be given in the following.

4.3. Example 3: three-dimensional mixed-mode SIFs

The model shown in Fig. 10(a) is still used while the load and boundary conditions are different. A centralized force $F_1 = 1$ is applied on the center of the top surface of the cylinder and the displacement boundary conditions are prescribed such that $u_1 = u_2 = u_3 = 0$ on the bottom surface. The following data and expressions are used for numerical analysis: $L = R = 200$; $a = 100$; $R_f = 10$; $E(x_2) = E_1 e^{\beta(x_2+L)}$; $\beta = \frac{1}{2L}\ln(E_2/E_1)$; $E_2/E_1 = 100$; $E_f/E_1 = 100$; $\nu = 0.25$; $K_0 = \sigma_F\sqrt{\pi a/Q}$; $\sigma_F = \frac{F_1}{\pi R^2}$.

Symmetry permits modeling of half cylinder as shown in Fig. 12. The mesh consists of 5792 elements and 25,728 nodes. Since the influence of the interface on the SIFs is focused, five domains ($R_I/R_e = 27, 36, 45, 54, 63$) shown in Fig. 11 are selected to compute the SIFs and only one of them does not contain the interface.

As shown in Fig. 13, the normalized SIFs K_I/K_0 and K_{II}/K_0 obtained at the angle ϕ and those at the angle $\pi - \phi$ are anti-symmetric, and K_{III}/K_0 at ϕ and those at $\pi-\phi$ are symmetric. It should be noted that the obtained mode-I SIFs K_{I} are negative when $\phi < \pi/2$, which implies two crack faces have been closed. According to Guo et al. (2008), only the positive K_{I} are meaningful and, however, the negative K_{I} can also be used in superposition with a positive K_{I} that results from another type of loading provided that the net K_{I} is positive. Therefore, presentation of the negative K_{I} can shed some light on the degree of closure occurring near the crack front region. In order to show the differences of the mixed-mode SIFs obtained in different integral domains clearly, the relative errors E_{rr} defined in Eq. (36) are shown in Fig. 14. It can be found that for all points along the crack front, the relative errors E_{rr} are within 0.15%, 0.85% and 0.90% for K_{I}/K_0, K_{II}/K_0 and K_{III}/K_0, respectively.

From Examples 2 and 3, it can be found that the material interfaces in the integral domain have almost no influence on the interaction integral, i.e., the interaction integral is domain-independent. The above three examples should be enough to illustrate the validation of the interaction integral method for extracting the SIFs in nonhomogeneous materials with complex interfaces.

5. Summary

In this paper, a new 3D domain expression of the interaction integral for extracting SIFs is derived. This expression does not contain any derivatives of material property parameters, and is still valid even when the integral domain contains material interfaces. This point is significant for solving the crack problems of nonhomogeneous materials with complex interfaces. The interaction integral method is combined with the FEM to analyze several representative fracture examples. It is found that the numerical results are in good agreement with those appearing in published papers. Moreover, the results show that interaction integral is domain-independent when the integral domain contains nonhomogeneous materials with continuous and discontinuous properties.

Acknowledgements

This work is sponsored by the Program of Excellent Team in Harbin Institute of Technology, Heilongjiang Province Foundation for Returned Scholars (LC2009C01), NSFC (10432030 and 10872056) and NCET (08-0151).

Appendix A

In the local curvilinear coordinate system as shown in Fig. 1, we select an arbitrary point p with the Cartesian coordinates (x_1,x_2,x_3) and its three curvilinear coordinates ξ_1, ξ_2 and ξ_3 are defined by the following relations:

$$\xi_1 = \mathbf{r}\cdot\mathbf{e}_1, \quad \xi_2 = \mathbf{r}\cdot\mathbf{e}_2, \quad \xi_3 = \int_0^s dl \tag{A1}$$

where the point s is on the crack front with minimum distance to point p, $\mathbf{r}$ is a position vector from the point s to p, $\mathbf{e}_1$ is a unit vector which is in the crack plane and perpendicular to the crack front, and $\mathbf{e}_2$ is a unit vector which is perpendicular to the crack plane. The corresponding natural base vectors $\mathbf{g}_i$ are defined by

$$\mathbf{g}_i = \frac{\partial x_k}{\partial \xi_i}\mathbf{i}_k \tag{A2}$$

The orthogonal unit base vectors $\mathbf{e}_i$ can be obtained by

$$\mathbf{e}_i = \mathbf{g}_i / B_{\underline{i}}, \quad B_{\underline{i}} = \sqrt{\mathbf{g}_{\underline{i}}\cdot\mathbf{g}_{\underline{i}}} \tag{A3}$$

where $\mathbf{e}_3$ is a unit vector tangent to the crack front.

The components of the auxiliary fields $\left(\boldsymbol{\sigma}^{\mathrm{aux}} = \sigma_{ij}^{\mathrm{aux}}\mathbf{e}_i\mathbf{e}_j,\ \boldsymbol{\varepsilon}^{\mathrm{aux}} = \varepsilon_{ij}^{\mathrm{aux}}\mathbf{e}_i\mathbf{e}_j \text{ and } \mathbf{u}^{\mathrm{aux}} = u_i^{\mathrm{aux}}\mathbf{e}_i\right)$ in (ξ_1,ξ_2,ξ_3) coordinate system can be defined as (Walters et al., 2006)

$$\sigma_{11}^{\mathrm{aux}} = \frac{1}{\sqrt{2\pi r}}\left[K_{\mathrm{I}}^{\mathrm{aux}}\cos\frac{\theta}{2}\left(1-\sin\frac{\theta}{2}\sin\frac{3\theta}{2}\right) - K_{\mathrm{II}}^{\mathrm{aux}}\sin\frac{\theta}{2}\left(2+\cos\frac{\theta}{2}\cos\frac{3\theta}{2}\right)\right] \tag{A4}$$

$$\sigma_{22}^{\mathrm{aux}} = \frac{1}{\sqrt{2\pi r}}\left[K_{\mathrm{I}}^{\mathrm{aux}}\cos\frac{\theta}{2}\left(1+\sin\frac{\theta}{2}\sin\frac{3\theta}{2}\right) + K_{\mathrm{II}}^{\mathrm{aux}}\sin\frac{\theta}{2}\cos\frac{\theta}{2}\cos\frac{3\theta}{2}\right] \tag{A5}$$

$$\sigma_{12}^{\mathrm{aux}} = \sigma_{21}^{\mathrm{aux}} = \frac{1}{\sqrt{2\pi r}}\left[K_{\mathrm{I}}^{\mathrm{aux}}\sin\frac{\theta}{2}\cos\frac{\theta}{2}\cos\frac{3\theta}{2} + K_{\mathrm{II}}^{\mathrm{aux}}\cos\frac{\theta}{2}\left(1-\sin\frac{\theta}{2}\sin\frac{3\theta}{2}\right)\right] \tag{A6}$$

$$\sigma_{13}^{\mathrm{aux}} = \sigma_{31}^{\mathrm{aux}} = -\frac{K_{\mathrm{III}}^{\mathrm{aux}}}{\sqrt{2\pi r}}\sin\frac{\theta}{2}, \quad \sigma_{23}^{\mathrm{aux}} = \sigma_{32}^{\mathrm{aux}} = \frac{K_{\mathrm{III}}^{\mathrm{aux}}}{\sqrt{2\pi r}}\cos\frac{\theta}{2} \tag{A7}$$

$$\sigma_{33}^{\mathrm{aux}} = \begin{cases} \nu(s)(\sigma_{11}^{\mathrm{aux}} + \sigma_{22}^{\mathrm{aux}}) & \text{plane strain} \\ 0 & \text{plane stress} \end{cases} \tag{A8}$$

$$u_1^{\mathrm{aux}} = \frac{1}{2\mu(s)}\sqrt{\frac{r}{2\pi}}\cdot\left[K_{\mathrm{I}}^{\mathrm{aux}}\cos\frac{\theta}{2}\left(\kappa_0 - 1 + 2\sin^2\frac{\theta}{2}\right) + K_{\mathrm{II}}^{\mathrm{aux}}\sin\frac{\theta}{2}\left(\kappa_0 + 1 + 2\cos^2\frac{\theta}{2}\right)\right] \tag{A9}$$

$$u_2^{\mathrm{aux}} = \frac{1}{2\mu(s)}\sqrt{\frac{r}{2\pi}}\cdot\left[K_{\mathrm{I}}^{\mathrm{aux}}\sin\frac{\theta}{2}\left(\kappa_0 + 1 - 2\cos^2\frac{\theta}{2}\right) - K_{\mathrm{II}}^{\mathrm{aux}}\cos\frac{\theta}{2}\left(\kappa_0 - 1 - 2\sin^2\frac{\theta}{2}\right)\right] \tag{A10}$$

$$u_3^{\mathrm{aux}} = \frac{1}{\mu(s)}\sqrt{\frac{2r}{\pi}}\cdot K_{\mathrm{III}}^{\mathrm{aux}}\sin\frac{\theta}{2} \tag{A11}$$

Here, $\kappa_0 = 3-4\nu(s)$ for plane strain and $\kappa_0 = [3-\nu(s)]/[1+\nu(s)]$ for plane stress at the point s on the crack front. Finally, the auxiliary strain fields are defined as

$$\varepsilon_{ij}^{\mathrm{aux}} = S_{ijkl}(\mathbf{x})\sigma_{kl}^{\mathrm{aux}} \tag{A12}$$

From the above definitions, the material properties used in the auxiliary stresses and displacements for any points are all identical to those evaluated at point s.

Appendix B

The details regarding Eq. (27) are as follows:

$$\begin{aligned}\boldsymbol{\sigma}^{\mathrm{aux}} : (\boldsymbol{\varepsilon}^{①} - \boldsymbol{\varepsilon}^{②})\mathbf{q}\cdot\mathbf{m} &= \boldsymbol{\sigma}^{\mathrm{aux}} : \left[(\nabla\mathbf{u})^{①} - (\nabla\mathbf{u})^{②}\right]\mathbf{q}\cdot\mathbf{m} \\ &= \sigma_{ij}^{\mathrm{aux}}\mathbf{e}_i\mathbf{e}_j : \frac{\mathbf{e}_l}{A_{\underline{l}}}\left\{\left[\frac{\partial(u_k\mathbf{e}_k)}{\partial\eta_l}\right]^{①} - \left[\frac{\partial(u_k\mathbf{e}_k)}{\partial\eta_l}\right]^{②}\right\}q_1 \\ &= \sigma_{ij}^{\mathrm{aux}}\mathbf{e}_j\cdot\frac{\delta_{il}}{A_{\underline{l}}}\left\{\left[\frac{\partial(u_k\mathbf{e}_k)}{\partial\eta_l}\right]^{①} - \left[\frac{\partial(u_k\mathbf{e}_k)}{\partial\eta_l}\right]^{②}\right\}q_1 \\ &= \sigma_{ij}^{\mathrm{aux}}\mathbf{e}_j\cdot\frac{1}{A_{\underline{l}}}\left[\left(\frac{\partial\mathbf{u}}{\partial\eta_l}\right)^{①} - \left(\frac{\partial\mathbf{u}}{\partial\eta_l}\right)^{②}\right]q_1\end{aligned} \tag{B1}$$

Appendix C

The numerator in Eq. (33) without body force can be written in tensor form as

$$\bar{I} = \int_V \{[\nabla\mathbf{u}\cdot\boldsymbol{\sigma}^{\mathrm{aux}} + \nabla\mathbf{u}^{\mathrm{aux}}\cdot\boldsymbol{\sigma} - \boldsymbol{\sigma}^{\mathrm{aux}} : \boldsymbol{\varepsilon}I] : (\mathbf{q}\nabla) + [\nabla\mathbf{u}\cdot(\boldsymbol{\sigma}^{\mathrm{aux}}\cdot\nabla) + (\nabla\mathbf{u}^{\mathrm{aux}}\nabla) : \boldsymbol{\sigma} - \nabla\boldsymbol{\sigma}^{\mathrm{aux}} : \boldsymbol{\varepsilon}]\cdot\mathbf{q}\}dV \tag{C1}$$

Since the auxiliary fields are defined in (ξ_1, ξ_2, ξ_3) coordinate system in Appendix A. In order to employ the interaction integral in finite element computations, Eq. (C1) is discretized in (ξ_1, ξ_2, ξ_3) coordinate system as

$$\bar{I} = \sum_{e=1}^{e_V} \sum_{p=1}^{p_e} \Big\{ \Big(\nabla_l u_i \sigma_{ij}^{\text{aux}} + \nabla_l u_i^{\text{aux}} \sigma_{ij} \Big) q_l \nabla_j - \sigma_{ij}^{\text{aux}} \varepsilon_{ij} q_l \nabla_l + \Big[\nabla_l u_i \sigma_{ij}^{\text{aux}} \nabla_j + \big(\nabla_l u_i^{\text{aux}} \nabla_j \big) \sigma_{ij} - \nabla_l \sigma_{ij}^{\text{aux}} \varepsilon_{ij} \Big] q_l \Big\}_p |\mathbf{J}|_p w_p \quad \text{(C2)}$$

Here, e_V is the number of elements in the integral domain V; p_e is the number of the integration points in one element; $|\mathbf{J}|_p$ represents the determinant of Jacobian matrix; w_p is the corresponding weight factor at the integration point p. Here, the variables marked by the subscripts i, j, k and l denote their components in (ξ_1, ξ_2, ξ_3) coordinate system.

In this paper, the unit vector $c_l(p)$ is in ξ_1 direction, i.e., $c_1 = 1$, $c_2 = c_3 = 0$. The nodal values $q_l^{n_I}$ of q_l on node n_I are given first and q_l is interpolated from their known nodal values $q_l^{n_I}$ by the expressions (Kim et al., 2001)

$$q_1(\xi) = \sum_{I=1}^{20} N_I(\xi) q_1^{n_I}, \quad q_2 = 0, \quad q_3 = 0 \quad \text{(C3)}$$

The value q_1 varies linearly in ξ_1 direction. The partial derivatives of q_l are

$$\frac{\partial q_1(\xi)}{\partial \xi_j} = \sum_{I=1}^{20} \frac{\partial N_I(\xi)}{\partial \xi_j} q_1^{n_I}, \quad \frac{\partial q_2}{\partial \xi_j} = 0, \quad \frac{\partial q_3}{\partial \xi_j} = 0 \quad \text{(C4)}$$

Therefore, the gradient of q_l is

$$q_l \nabla_j = \frac{1}{B_{\underline{j}}} \frac{\partial q_l}{\partial \xi_j} + \frac{q_i}{B_{\underline{j}}} \Gamma_{ij,l} \quad \text{(C5)}$$

where $B_{\underline{i}}$ is given in Appendix A and $\Gamma_{ij,l}$ is defined by

$$\frac{\partial \mathbf{e}_i}{\partial \xi_j} = \Gamma_{ij,l} \mathbf{e}_l \quad \text{(C6)}$$

Similarly to the gradient of q_l in Eq. (C5), the gradients of auxiliary fields and actual fields ($\nabla_l u_i^{\text{aux}}$, $\nabla_l u_i^{\text{aux}} \nabla_j$, $\nabla_l \sigma_{ij}^{\text{aux}}$ and $\nabla_l u_i$) can be solved.

According to Eq. (11), the denominator in Eq. (33) can be obtained by

$$\int_{L_c} \Delta a(p)\, dl = \int_{L_c} q_1\, dl. \quad \text{(C7)}$$

References

Ayhan, A.O., 2007. Stress intensity factors for three-dimensional cracks in functionally graded materials using enriched finite elements. International Journal of Solids and Structures 44 (25–26), 8579–8599.

Ayhan, A.O., 2009. Three-dimensional mixed-mode stress intensity factors for cracks in functionally graded materials using enriched finite elements. International Journal of Solids and Structures 46, 796–810.

Ayhan, A.O., Nied, H.F., 2002. Stress intensity factors for three-dimensional surface cracks using enriched finite elements. International Journal for Numerical Methods in Engineering 54, 899–921.

Birman, V., Byrd, L.W., 2007. Modeling and analysis of functionally graded materials and structures. Applied Mechanics Reviews 60, 195–216.

DeLorenzi, H.G., 1982. On the energy release rate and the J-integral for 3-D crack configurations. International Journal of Fracture 19, 183–193.

Dolbow, J.E., Gosz, M., 2002. On the computation of mixed-mode stress intensity factors in functionally graded materials. International Journal of Solids and Structures 39, 2557–2574.

Eischen, J.W., 1987. Fracture of nonhomogeneous materials. International Journal of Fracture 34, 3–22.

Gosz, M., Moran, B., 2002. An interaction energy integral method for computation of mixed-mode stress intensity factors along non-planar crack fronts in three dimensions. Engineering Fracture Mechanics 69, 299–319.

Gosz, M., Dolbow, J., Moran, B., 1998. Domain integral formulation for stress intensity factor computation along curved three-dimensional interface cracks. International Journal of Solids and Structures 35 (15), 1763–1783.

Gravouil, A., Moës, N., Belytschko, T., 2002. Non-planar 3D crack growth by the extended finite element and level sets. Part II: level set update. International Journal for Numerical Methods in Engineering 53, 2569–2586.

Guo, L.C., Noda, N., Wu, L.Z., 2008. Thermal fracture model for a functionally graded plate with a crack normal to the surfaces and arbitrary thermomechanical properties. Composites Science and Technology 68, 1034–1041.

Honein, T., Herrmann, G., 1997. Conservation laws in nonhomogeneous plane elastostatics. Journal of the Mechanics and Physics of Solids 45 (5), 789–805.

Irwin, G.R., 1962. Crack extension force for a part-through crack in a plate. Journal of Applied Mechanics 29 (4), 651–654.

Jin, Z.H., Sun, C.T., 2007. Integral representation of energy release rate in graded materials. Journal of Applied Mechanics 74, 1046–1048.

Johnson, J., Qu, J.M., 2007. An interaction integral method for computing mixed-mode stress intensity factors for curved bimaterial interface cracks in non-uniform temperature fields. Engineering Fracture Mechanics 74, 2282–2291.

Kim, J.H., Paulino, G.H., 2003. T-stress, mixed-mode stress intensity factors, and crack initiation angles in functionally graded materials: a unified approach using the interaction integral method. Computer Methods in Applied Mechanics and Engineering 192, 1463–1494.

Kim, J.H., Paulino, G.H., 2004. T-stress in orthotropic functionally graded materials: Lehnitskii and Stroh formalisms. International Journal of Fracture 126, 345–384.

Kim, J.H., Paulino, G.H., 2005. Consistent formulations of the interaction integral method for fracture of functionally graded materials. Journal of Applied Mechanics 72, 351–364.

Kim, Y.J., Kim, H.G., Im, S., 2001. Mode decomposition of three-dimensional mixed-mode cracks via two-state integrals. International Journal of Solids and Structures 38, 6405–6426.

Krysl, P., Belytschko, T., 1999. The element-free Galerkin method for dynamic propagation of arbitrary 3-D cracks. International Journal for Numerical Methods in Engineering 44, 767–800.

Leggoe, J.W., Hu, X.Z., Bush, M.B., 1996. Crack tip damage development and crack growth resistance in particulate reinforced metal matrix composites. Engineering Fracture Mechanics 53 (6), 873–895.

Moës, N., Gravouil, A., Belytschko, T., 2002. Non-planar 3D crack growth by the extended finite element and level sets. Part I: mechanical model. International Journal for Numerical Methods in Engineering 53, 2549–2568.

Moran, B., Shih, C.F., 1987a. A general treatment of crack tip contour integrals. International Journal of Fracture 35, 295–310.

Moran, B., Shih, C.F., 1987b. Crack tip and associated domain integrals from momentum and energy balance. Engineering Fracture Mechanics 27 (6), 615–642.

Nahta, R., Moran, B., 1993. Domain integrals for axisymmetric interface crack problems. International Journal of Solids and Structures 30 (15), 2027–2040.

Nakamura, T., 1991. Three-dimensional stress fields of elastic interface cracks. Journal of Applied Mechanics 58, 939–946.

Nakamura, T., Parks, D.M., 1988. Three-dimensional stress field near the crack front of a thin elastic plate. ASME Journal of Applied Mechanics 55, 805–813.

Ortiz, J.E., Cisilino, A.P., 2005. Boundary element method for J-integral and stress intensity factor computations in three-dimensional interface cracks. International Journal of Fracture 133, 197–222.

Ozturk, M., Erdogan, F., 1996. Axisymmetric crack problem in bonded materials with a graded interfacial region. International Journal of Solids and Structures 33 (2), 193–219.

Pook, L.P., 1994. Some implications of corner point singularities. Engineering Fracture Mechanics 48 (3), 367–378.

Rahman, S., Chakraborty, A., 2007. A stochastic micromechanical model for elastic properties of functionally graded materials. Mechanics of Materials 39, 548–563.

Raju, I.S., Newman, J.C., 1979. Stress–intensity factors for a wide range of semi-elliptical surface cracks in finite-thickness plates. Engineering Fracture Mechanics 11, 817–829.

Rice, J.R., 1968. A path independent integral and the approximate analysis of strain concentration by notches and cracks. Journal of Applied Mechanics 35, 379–386.

Shah, R.C., Kobayashi, A.S., 1972. On the surface flaw problem. In: Swcdlow, J.L. (Ed.), The Surface Crack: Physical Problems and Computational Solutions. ASME, New York, pp. 79–124.

Shih, C.F., Moran, B., Nakamura, T., 1986. Energy release rate along a three-dimensional crack front in a thermally stressed body. International Journal of Fracture 30, 79–102.

Smith, F.W., 1972. The elastic analysis of the part-circular surface flaw problem by the alternating method. In: Swcdlow, J.L. (Ed.), The Surface Crack: Physical Problems and Computational Solutions. ASME, New York, pp. 125–152.

Smith, F.W., Emery, A.F., Kobayashi, A.S., 1967. Stress intensity factors for semicircular cracks. Part 2: semi-infinite solid. Journal of Applied Mechanics 34, 947–952.

Stern, M., Becker, E.B., Dunham, R.S., 1976. A contour integral computation of mixed-mode stress intensity factors. International Journal of Fracture 12 (3), 359–368.

Sukumar, N., Moran, B., Black, T., Belytschko, T., 1997. An element-free Galerkin method for three-dimensional fracture mechanics. Computational Mechanics 20, 170–175.

Sukumar, N., Moës, N., Moran, B., Belytschko, T., 2000. Extended finite element method for three-dimensional crack modelling. International Journal for Numerical Methods in Engineering 48, 1549–1570.

Walters, M.C., Paulino, G.H., Dodds, R.H., 2004. Stress–intensity factors for surface cracks in functionally graded materials under mode-I thermomechanical loading. International Journal of Solids and Structures 41, 1081–1118.
Walters, M.C., Paulino, G.H., Dodds, R.H., 2005. Interaction integral procedures for 3-D curved cracks including surface tractions. Engineering Fracture Mechanics 72, 1635–1663.
Walters, M.C., Paulino, G.H., Dodds, R.H., 2006. Computation of mixed-mode stress intensity factors for cracks in three-dimensional functionally graded solids. Journal of Engineering Mechanics 132 (1), 1–15.
Wang, S.S., Yau, J.F., Corten, H.T., 1980. A mixed-mode crack analysis of rectilinear anisotropic solids using conservation laws of elasticity. International Journal of Fracture 16 (3), 247–259.
Yang, L.H., Li, Z.H., 2004. The interaction of mode-I crack with multi-inclusions in a three-phase model. International Journal of Fracture 127, 193–200.
Yildirim, B., Dag, S., Erdogan, F., 2005. Three-dimensional fracture analysis of FGM coatings under thermomechanical loading. International Journal of Fracture 132, 369–395.
Yu, H.J., Guo, L.C., Wu, L.Z., 2007. Numerical investigation on the fracture behaviors of three-dimensional functionally graded materials. Key Engineering Materials, 1098–1101.
Yu, H.J., Wu, L.Z., Guo, L.C., Du, S.Y., He, Q.L., 2009. Investigation of mixed-mode stress intensity factors for nonhomogeneous materials using an interaction integral method. International Journal of Solids and Structures 46, 3710–3724.